Effect of Martensite Start and Finish Temperature on Residual Stress Development in Structural Steel Welds

The experimental electrodes with lower Cr-Ni contents were found capable of promoting compressive residual stresses in welds

BY M. C. PAYARES-ASPRINO, H. KATSUMOTO, AND S. LIU

ABSTRACT. Martensite start and finish temperatures are very important in structural steel welding because they control the residual stresses in a weld. Tensile residual stresses amplify the effect of applied tensile stress. On the other hand, compressive residual stresses are algebraically added to the applied tensile stresses to result in a lower net stress level experienced by a weld, thus inhibiting crack initiation and increasing the fatigue life of the welded component.

The residual stress state, i.e., whether compressive or tensile, and its magnitude will depend on the expansion that accompanies the austenite-to-martensite transformation and the thermal shrinkage due to cooling. High martensite start temperature and low martensite finish temperature will both minimize the effect of transformation-induced compressive stress generation. To obtain a full martensitic structure in a weld metal within an optimal range of temperatures will depend mainly on the filler metal composition. A new type of welding wire capable of inducing a local compressive residual stress state by means of controlled martensitic transformation at relatively low temperatures has been studied.

In this study, several low-transformation-temperature welding (LTTW) wires have been developed and investigated to determine the martensite start and finish temperatures of the welds. Also studied was the effect of the martensite start and finish temperatures on microstructural development and hardness in single- and multi-pass weldments.

Introduction

It is well known that high tensile residual stresses near a weld decrease the fatigue performance of the weld because these initial stresses, when superimposed on the applied stresses, elevate the overall mean stress (Refs. 1–4). Several procedures have been developed to relieve the tensile residual stresses in welded joints. Postweld heat treatment (PWHT) and shot peening are two common methods used to improve fatigue properties (Ref. 3). Another way to reduce or eliminate undesirable residual stresses in welded parts is to modify the welding process itself. For example, low heat input and small weld pool are known to reduce residual stress. Physical and mechanical properties such as heat capacity, density, thermal expansion coefficient, and strength of the base metal and filler metal contribute to the magnitude of the residual stresses generated in a weld (Refs. 4–6).

It has long been recognized that phase transformations in steels can radically affect the development of residual stresses. For example, Jones and Alberry (Ref. 7) showed how transformation temperatures influence the evolution of stress as a constrained sample cools from the austenite state. It is significant that their experiments showed that the residual stress at ambient temperature is smaller when the transformation temperature is reduced.

Ohta et al. (Ref. 8) designed a welding alloy containing 10% Cr and 10% Ni, with an exceptionally low austenite-to-martensite transformation temperature, T_{Ms}. In this alloy, martensitic transformation in an unconstrained specimen starts at about 180°C and ends right at ambient temperature. By contrast, normal steel welding alloys have transformation temperatures around 400°–500°C. As illustrated in Fig. 1A, the net strain on cooling between T_{Ms} and ambient temperature is contraction in the case of the conventional alloy, whereas there is a net expansion for the new welding wire. As such, local tensile residual stress results in the conventional wire and compressive residual stress for the low-Ms alloy at ambient temperature — Fig. 1B.

When fatigue tests were conducted on welded sections, the structures joined using the low-Ms alloy weld metal exhibited much higher fatigue strength (Ref. 8). This improvement of approximately 20% is attributed to the compressive residual stress, which reduces the effective stress range that the structure experiences during fatigue testing (Ref. 8). The achievement is based entirely on the fact that the reduction of the transformation temperature allows the expansion originated from martensite transformation to compensate for the accumulated thermal contraction strains. The improved results and the substantial benefits are expected to bring radical changes in fatigue design philosophies for structural components. This effect has recently been confirmed by Eckerlid et al. (Ref. 9), Martinez Diez (Refs. 10, 11), and Darcis et al. (Ref. 24).

KEYWORDS

Martensitic Transformation
Martensite Start Temperature
Low Transformation Temperature Welding Electrodes
LTTW Electrodes
Weld Metal Phase Transformations
Compressive Residual Stress
Dilatometric Measurements
Consumable Development

Low-Transformation-Temperature Welding (LTTW) Wires

Martensitic Transformation Approach

Martensitic Transformation — Volume Change and Residual Stress

The principal decomposition products of austenite during cooling are precipitated phases that include carbides and nitrides, or the polymorphic phases of al-

M. C. PAYARES-ASPRINO is with Universidad Simón Bolivar, Caracas, Venezuela. H. KATSUMOTO is with Sumitomo Metal Industries, Ltd., Kashima-City, Ibaraki, Japan. S. LIU is with Colorado School of Mines, Golden, Colo.

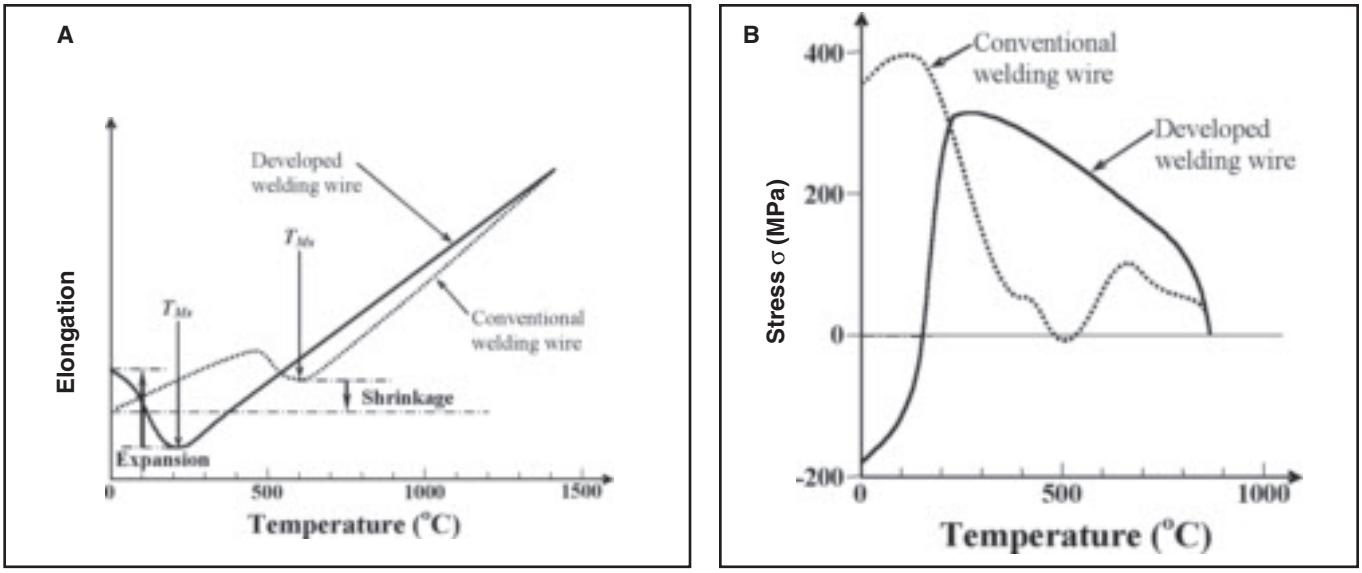

Fig. 1 — Comparison between the designed low-T_{Ms} wire (10% Cr-10% Ni) and conventional steel wire. A — Transformation of weld metal during unconstrained cooling; B — development of stress during constrained cooling (Ref. 8).

loyed iron, which includes the low-temperature ferrite (α) and the diffusionless transformation products, BCT α-martensite, and HCP ε-martensite (Ref. 12). The BCT martensite phase can be thought of as a variant of the thermodynamically favored α-ferrite, which would have formed from the austenite upon cooling were it not for the severe limitation of the diffusional processes due to fast cooling (Ref. 13). In the absence of ferrite formation by nucleation and growth, austenite undergoes the much more dynamic martensite transformation, involving short-range atomic rearrangements over broad interfaces at high velocity. The diffusionless shear-type martensitic transformation requires considerably greater driving force than the diffusion-controlled growth of ferrite in austenite, due to mechanical shearing of the austenite lattice. Consequently, martensitic transformation usually requires a considerably greater undercooling below the equilibrium temperature, T_0, at which the parent and transformed phases are in thermodynamic equilibrium. The relative stability of the austenite phase is very important in order to induce martensitic transformation at a desired temperature or stress level. The strain due to phase transformation can alter the state of residual stress or strain. It is well known that the martensitic transformation of the carburized surface of a steel component puts the surface under compression as a result of the expansion at the surface due to the formation of the lower-density martensite from austenite.

Table 1 — Compositions of the Welds (in wt-%) Produced Using the CSM Experimental Metal-Cored Wires

Wires	C	Mn	Cr	Ni	P	Mo	Si	S	Ti
Al	0.04	0.89	10.00	0.30	<0.01	0.04	0.20	<0.01	<0.01
A6	0.08	0.89	14.70	0.27	<0.01	0.04	0.19	<0.01	<0.01
B5	0.04	0.86	13.00	1.70	<0.01	0.04	0.16	<0.01	<0.01
C5	0.05	0.41	3.00	13.2	<0.01	0.35	0.22	<0.01	<0.01
ER70S-3	0.09	1.02	0.05	0.03	<0.01	<0.01	0.41	<0.01	<0.01

Table 2 — Transformation Temperatures Measured Using Dilatometry

Wire	Ac_1	Ac_3	Ar_3 (T_{Ms}, T_{Fs})[a]	A_{r1} (T_{Mf},T_{Ff})[a]	ε_f(%)[b]
A1	800	850	390	284	0.244
A6	790	815	360	190	0.081
B5	740	780	300	225	0.416
C5	635	720	270	120	0.570
ER70S-3	820	860	645	580	–0.570

(a) T_{Ms} and T_{Mf} are for A1, A6, B5, and C5.
T_{Fs} and T_{Ff} are for ER70S-3
(b) The final strain (ε_f) is defined as the amount of expansion from the T_{Ms} of T_{Fs} temperature to the room temperature. Positive means an expansive strain exists at room temperature, negative means a contractive strain exists.

Martensitic Transformation Temperature

Martensite transformation begins at martensite start temperature, T_{Ms}, (Fig. 1), which can vary over a wide temperature range, from as high as 500°C to well below room temperature, depending on the concentration of γ-stabilizing alloying elements in the steel. Once T_{Ms} is reached, martensite begins to form with further transformation taking place during cooling until reaching the martensite finish temperature, T_{Mf} — Fig. 1. At this temperature, all the austenite should have transformed to martensite, but frequently in practice, a small portion of the austenite remains untransformed even at low temperatures. Large volume fractions of austenite can be retained in some highly alloyed steels, where the T_{Mf} temperature is well below room temperature.

To achieve martensitic transformation, it is usually necessary for the steel to be cooled rapidly, fast enough to suppress the higher temperature, diffusion-controlled

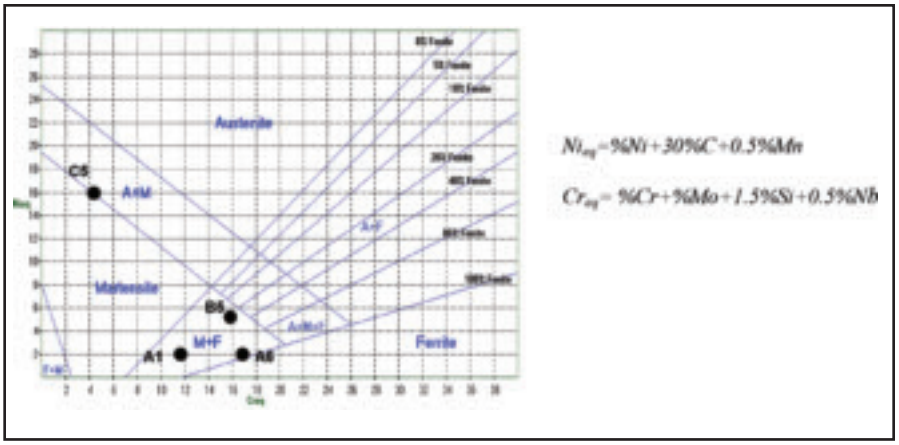

Fig. 2 — Compositions of the welds plotted on the Schaeffler diagram.

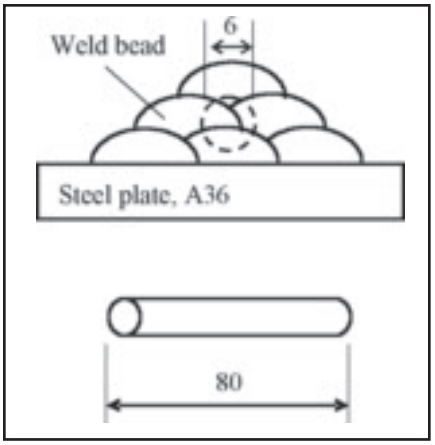

Fig. 3 — Cylindrical specimens according to the Gleeble standard specimen were extracted from the welds. (All dimensions are given in mm.)

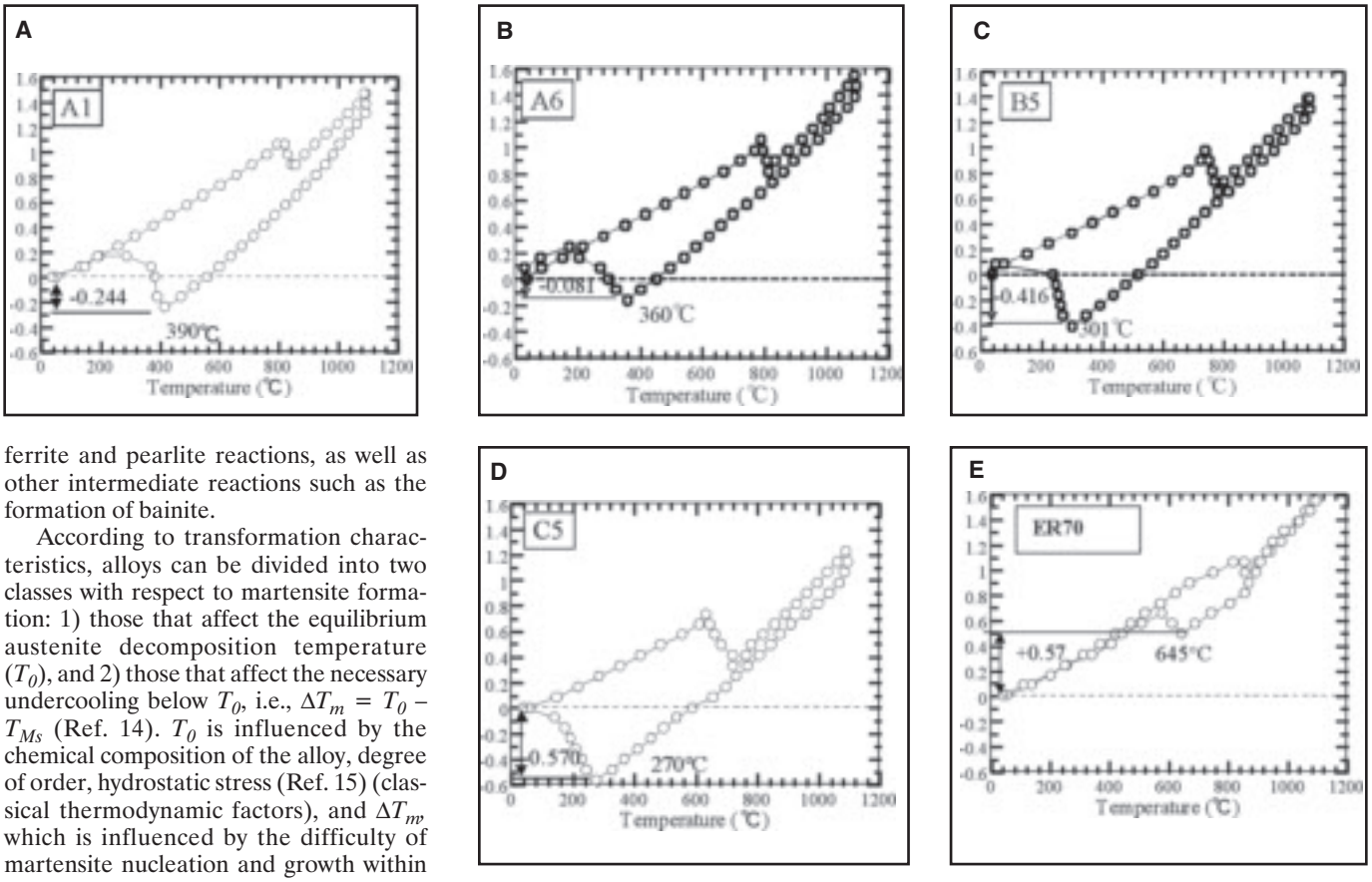

Fig. 4 — Dilatometric curves of the welds made using the experimental wires and commercial wire.

ferrite and pearlite reactions, as well as other intermediate reactions such as the formation of bainite.

According to transformation characteristics, alloys can be divided into two classes with respect to martensite formation: 1) those that affect the equilibrium austenite decomposition temperature (T_0), and 2) those that affect the necessary undercooling below T_0, i.e., $\Delta T_m = T_0 - T_{Ms}$ (Ref. 14). T_0 is influenced by the chemical composition of the alloy, degree of order, hydrostatic stress (Ref. 15) (classical thermodynamic factors), and ΔT_m, which is influenced by the difficulty of martensite nucleation and growth within the austenite matrix (kinetic, activation factor). The factors that affect the ΔT_m include external shear stresses and any other products that may affect the resistance of the base austenite lattice to mechanical shear during martensite transformation, e.g., hardening mechanism, point defects, dislocations, and precipitates.

Martensite Formation — Influence of Alloying Elements

The effect of alloying elements on the T_{Ms} temperature has been studied by many researchers. Izumiyama et al. (Ref. 16) showed the effects of individual alloying of 13 elements. Their results showed that Al, Ti, V, Nb, and Co effectively increased the T_{Ms}, whereas Si, Cu, Cr, Ni, Mn, and C decreased the T_{Ms} temperature. However, Liu (Ref. 17) reported different effects for some of the elements. He showed that all alloying elements mentioned earlier (Mn, V, Cr, Cu, W, Si), except Al and Co, decreased the T_{Ms} temperature. The different observations are not unexpected since different processing conditions (e.g., austenitizing conditions and cooling rates), austenite grain size, and impurity content will significantly af-

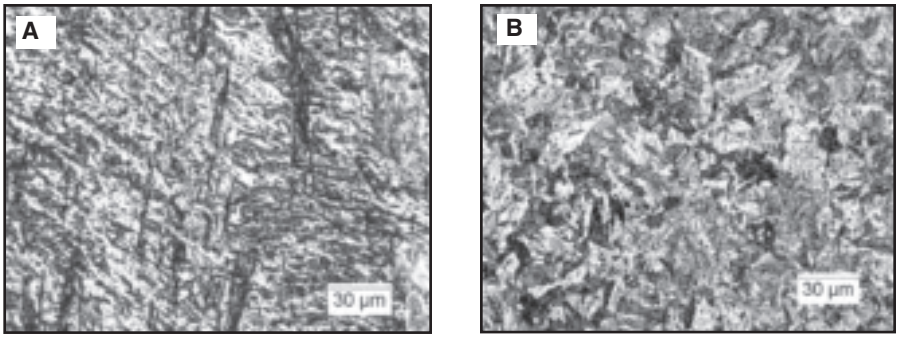

Fig. 5 — Microstructures of A1 in single-pass weld bead and Gleeble specimen. A — Single-pass weld bead; B — Gleeble specimen.

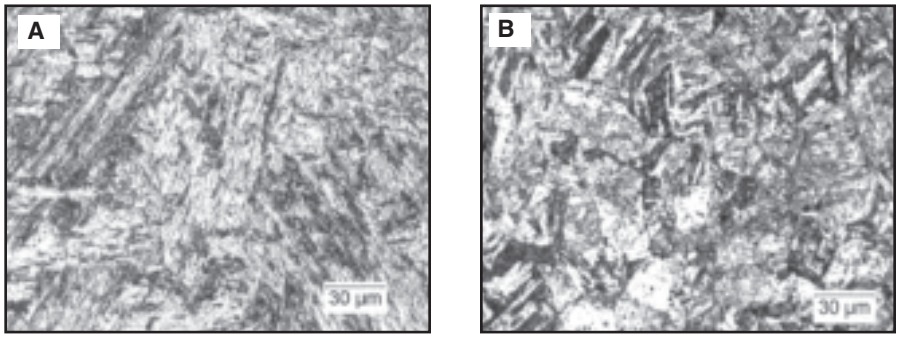

Fig. 6 — Microstructures of A6 in single-pass weld bead and Gleeble specimen. A — Single-pass weld bead; B — Gleeble specimen.

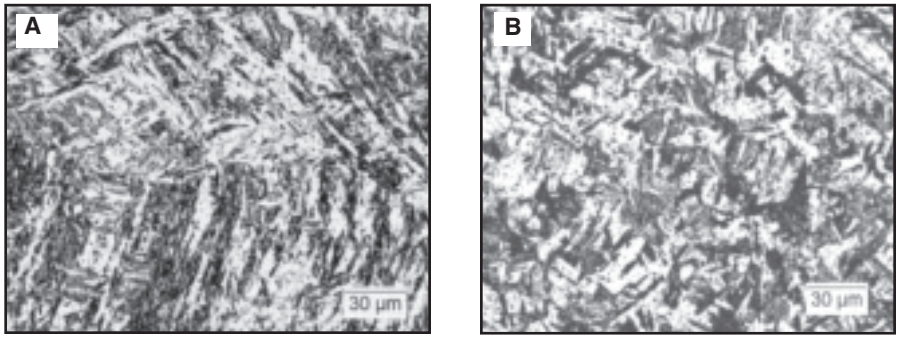

Fig. 7 — Microstructures of B5 in single-pass weld bead and Gleeble specimen. A — Single-pass weld bead; B — Gleeble specimen.

Table 3 — Experimentally Measured and Calculated Martensite Start Temperatures of Weld Metal

Wires	Experimental T_{Ms} (C°)	Self-Olson Equation T_{Ms} (C°)	Ghosh and Olson T_{Ms} (C°±400)
A1	416	334	332
A6	360	280	325
B5	301	260	318
C5	279	175	291
ER70S-3	620[a]	—	—

(a) Ferrite transformation start temperature (T_{Fs}).

fect the martensite transformation behavior. All these metallurgical factors need to be carefully considered in order to manage the martensite transformation behavior of an alloy.

This paper describes the development and characterization of several LTTW consumables that contained lower combined alloy contents (than the 10% Cr and 10% Ni developed by Ohta et al. (Ref. 8)) for the management of weld residual stresses and improvement of weld joint fatigue properties. Metal cored electrodes were manufactured and welds prepared. The welds were analyzed for chemical composition and specimens were extracted for dilatometric analysis for T_{Ms} determination. The welds were also cross-sectioned for metallography and hardness testing.

Experimental Procedures

Chemical Composition of the Weld

The CSM-designed filler metal produced ferrite-martensite and ferrite-austenite microstructure. The composition of the welds produced using the four metal-cored welding wires are shown in Table 1.

The chromium and the nickel equivalents of each of the welds were calculated and plotted on the Schaeffler diagram as shown in Fig. 2. A1, A6, and B5 are expected to result in a ferrite–martensite microstructure while C5 is expected to be martensitic with some retained austenite.

For comparison, a commercial solid wire, AWS ER70S-3, was also included in the research. Two models were used to calculate the martensite start temperatures of these alloys, the Self-Olson Equation (Refs. 18, 19) and the methodology proposed by Ghosh and Olson (Refs. 20–22). Scanning electron microscopy (SEM) and energy-dispersive spectroscopy (EDS) were used to examine the microstructure as well as alloying element segregation in the welds.

Dilatometric Measurements

Dilatometric specimens were extracted from single-pass welds deposited on an A36 grade structural steel using the four experimental consumables and the commercial ER70S-3 wire. The dilatometric measurements were made on a Gleeble thermomechanical simulator (Fig. 3) using 6-mm-diameter and 80-mm-length samples. The small cylinders were heated at the rate of 10°C/s to 1050°C and held at that temperature for 3 min, followed by quenching in a helium jet at the cooling rate of 100°C/s.

Microstructural Development

The specimens were prepared to a mirror-finish using standard metallographic techniques and etched with the Kalling No. 2 reagent (1.5 g $CuCl_2$ + 33 mL HCl + 33 mL ethanol + 33 mL H_2O) according to ASTM E407 and E340 testing techniques. Photomicrographs were taken using a LECO Olympus PMG-3 field microscope, coupled to a PaxCAM camera. Area fractions of martensite and ferrite were measured using the point counting technique.

Microhardness Distribution in the Weldments

Microhardness testing was conducted on transverse cross sections taken from the welds. Measurements were made on a Vickers microhardness scale with a load of 300 g. The objective of this study was to evaluate the hardness of single- and multipass welds; both as-solidified and reheated zones were measured. In the case of multipass welds, measurements were made in the "No-Reheat" (as-solidified) zone, "Once-Reheated" (reheated weld metal) zone, and "Twice-Reheated" (overlapping reheated) zones.

Samples for microhardness testing were first etched to identify the weld fusion zone. Hardness measurements were made across the weld interface at two different distances from the surface of the last bead of the weldments. Indentations were made at increments of 0.3175 mm inside the weld metal. However, the increments between successive measurements were reduced to 0.1588 mm when approaching the reheated zones in order to detect changes in hardness in these areas.

Results and Analysis

Results from the dilatometric analysis and microstructural analysis are presented and discussed in the following.

Dilatometric Analysis

The dilatometric curves and the martensite start temperature data are presented. In addition, the experimentally determined values are compared with the predicted values using the Self-Olson equations and the Ghosh-Olson methodology.

Dilatrometric Curves

Figure 4 shows the dilatometric curves for the four designed and conventional wires obtained using the Gleeble thermomechanical simulator. Martensitic transformation occurred in all four designed wires. The martensite start temperature and the relative strain (compressive or tensile) are recorded on each of the figures. Data from the C5 sample was selected for further description and interpretation of the dilatometric measurements. At the beginning of the test, the percent strain was zero. With increasing temperature, the sample began to expand as evidenced by the positive strain. Ferrite-to-austenite transformation ($\alpha \rightarrow \gamma$) began at approximately 635°C and ended at around 720°C, representing a deviation from the equilibrium Ac1 and Ac3 temperatures. The negative slope during $\alpha \rightarrow \gamma$ transformation indicates contraction because of the denser atomic packing factor of austenite. After the holding temperature of 1050°C, the sample was allowed to cool down at the rate of 100°C/s and contraction was observed. At 270°C, the slope began to change again indicating that martensite began to form. Up to this point, cooling has amounted to a contraction of about 1.8% (from +1.2 to

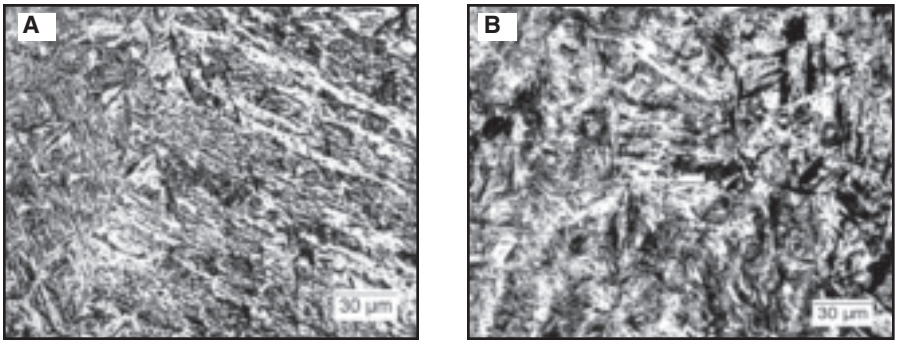

Fig. 8 — Microstructures of C5 in single-pass weld bead and Gleeble specimen. A — Single-pass weld bead; B — Gleeble specimen.

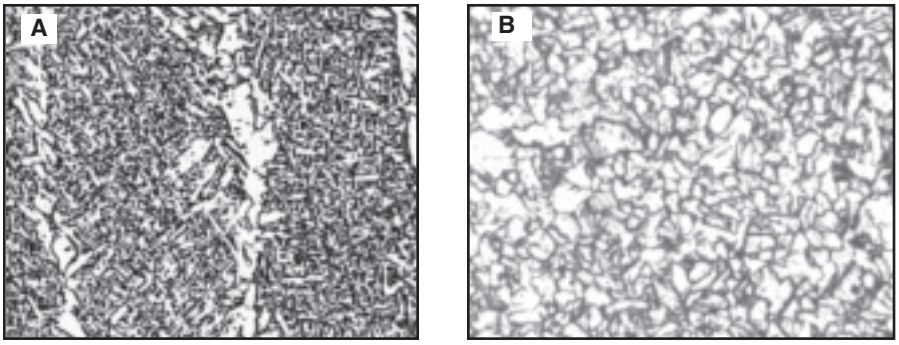

Fig. 9 — Microstructures of ER70S-3. A — Single-pass weld bead; B — Gleeble specimen.

Table 4 — Microstructure (in vol-%) of Single-Pass Welds and Gleeble Specimens

	A1 Wire		A6 Wire		B5 Wire		C5 Wire	
Volume %	SP-A1	G-A1	SP-A6	G-A6	SP-B5	G-B5	SP-C5	G-C5
Carbides	72.6	70.4	62.0	63.2	70.5	70.1	83.4	75.1
Matrix	27.4	29.5	38.0	36.8	29.5	30.0	16.6	24.9

Table 5 — Average Hardness Readings of Single-Pass Welds and the Gleeble Specimens

Hardness	A1 Wire		A6 Wire		B5 Wire		C5 Wire	
Specimen	SP-A1	G-A1	SP-A6	G-A6	SP-B5	G-B5	SP-C5	G-C5
HV_{300}	386	352	337	337	375	375	400	393

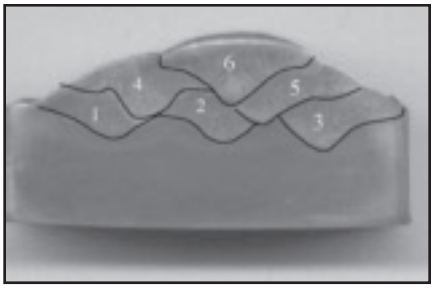

Fig. 10 — Macrophotograph of weld B5 showing the three layers and six weld beads.

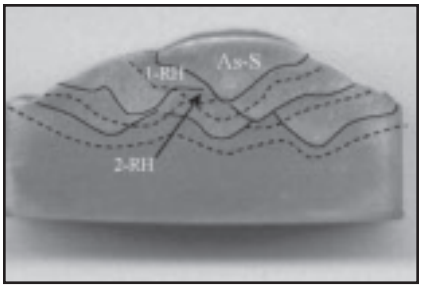

Fig. 11 — Macrophotograph of the multipass weld B5 with lines designating the different weld zones: as-solidified weld metal, once-reheated zone, and twice-reheated zone.

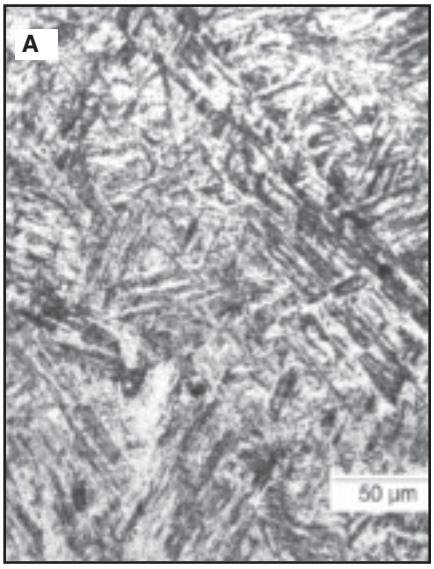

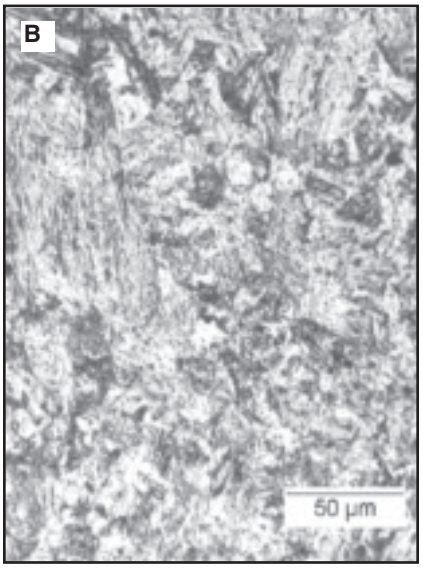

Fig. 12 — Microstructures of as-solidified and once-reheated areas. A — As-solidified fifth pass; B — once-reheated fourth pass.

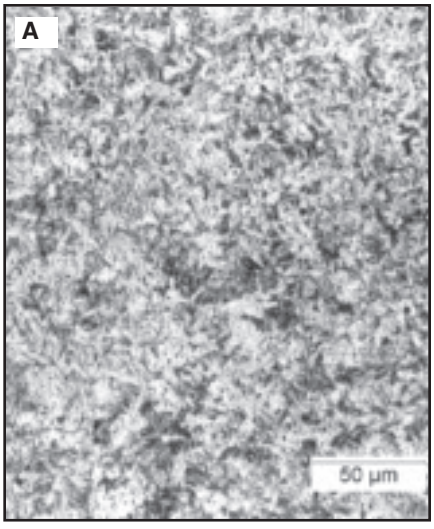

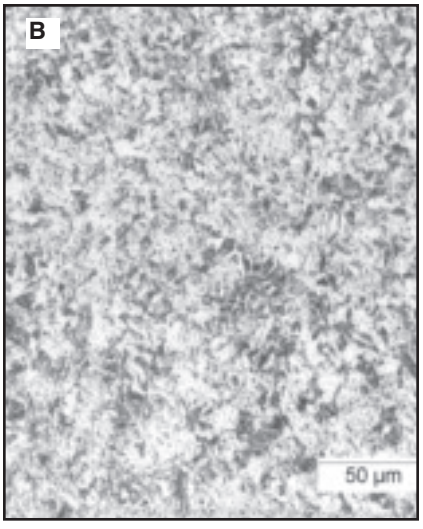

Fig. 13 — Microstructure of twice-reheated areas in weld A1. A — Twice reheated with the fifth and sixth passes; B — twice reheated with the fourth and sixth passes.

–0.6%). Assuming that the welded structure was entirely rigid, the contraction of austenite would have resulted in tensile residual stresses. However, with the formation of martensite and its more open body-centered tetragonal (BCT) crystal structure, the contraction reversed to expansion. Finally, at room temperature, the strain reached around zero.

The martensite transformation start temperature (T_{Ms}) is identified as the temperature at which the slope changed from positive to negative during cooling. Similarly, the martensite transformation finish temperature (T_{Mf}) can be identified as the temperature when the negative slope turned to positive. Even though it is not necessary for all the austenite to decompose into martensite at M_f to control residual stress, the magnitude of the expansion is important since it is responsible for offsetting the residual tensile stress state that originated from thermal contraction.

Sample C5 exhibited the lowest T_{Ms} temperature and the largest amount of expansion. The expansive strain also remained at room temperature. These results indicate that compressive residual stresses can be induced in the vicinity of the weld metal in a welded joint produced using the C5 welding wire.

Martensite transformation initiated in sample A1 at 390°C and the amount of expansion was around 0.5% (from –0.3% to 0.2%). Nevertheless, the martensite transformation completed at a relatively high temperature, around 284°C. Thus, a part of the effect of expansion would be offset by subsequent cooling and contraction of thermal origin. The overall strain (ε_f) for sample A1, measured from the onset of martensitic transformation to room temperature, was only 0.244% as indicated in Fig. 4. It is clear by comparing sample C5 with A1 that the onset and the end of martensite transformation are just as important as the magnitude of the expansion in controlling the final residual stress state in a welded joint. For comparison, the T_{Ms}, T_{Mf}, and ε_f of sample A6 are 360°C, 190°C, and 0.244%, respectively. For sample B5, these values are 300°C, 225°C, and 0.578%. Lower T_{Ms} and T_{Mf}, and larger ε_f will maximize the compressive residual stress in a welded joint.

On the contrary, a phase transformation was observed to start at 645°C and finished at 580°C during cooling in sample ER70S-3. Microscopic observation concluded that ferrite transformation occurred instead of martensite transformation. The lower alloying content of this welding wire certainly supports this observation. After the transformation, cooling has amounted to a contraction of 0.57% and then the strain reached around zero at room temperature. These measurements

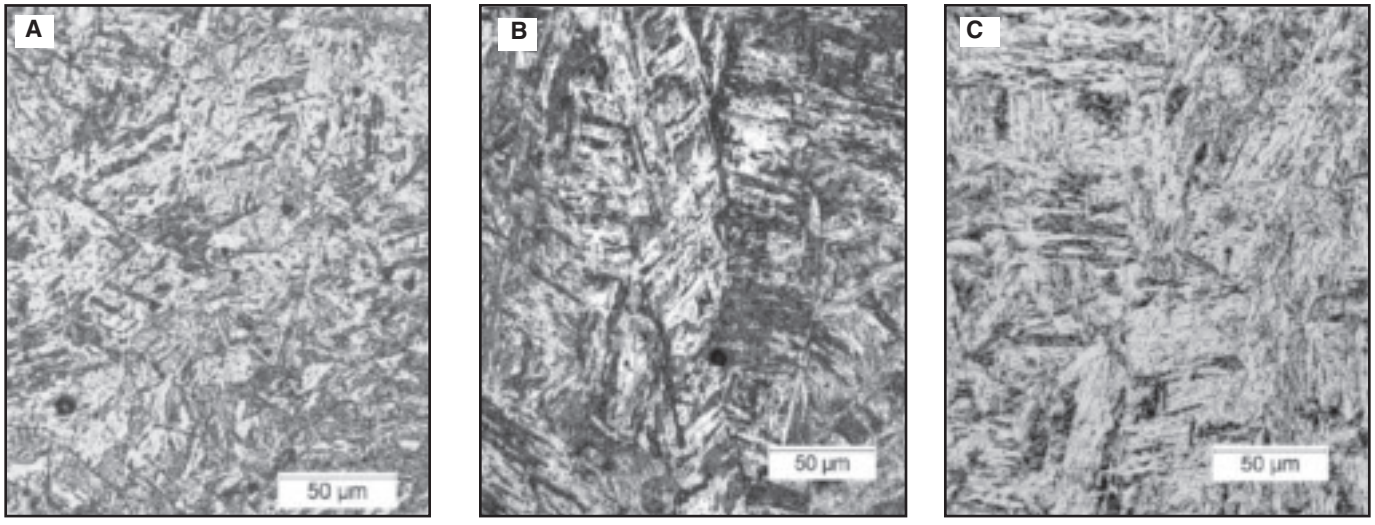

Fig. 14 — Microstructure of as-solidified first, second, and third passes in weld A6. A — As-solidified in the first pass, HV398; B — as-solidified in the second pass, HV375; C — as-solidified in the third pass, HV380.

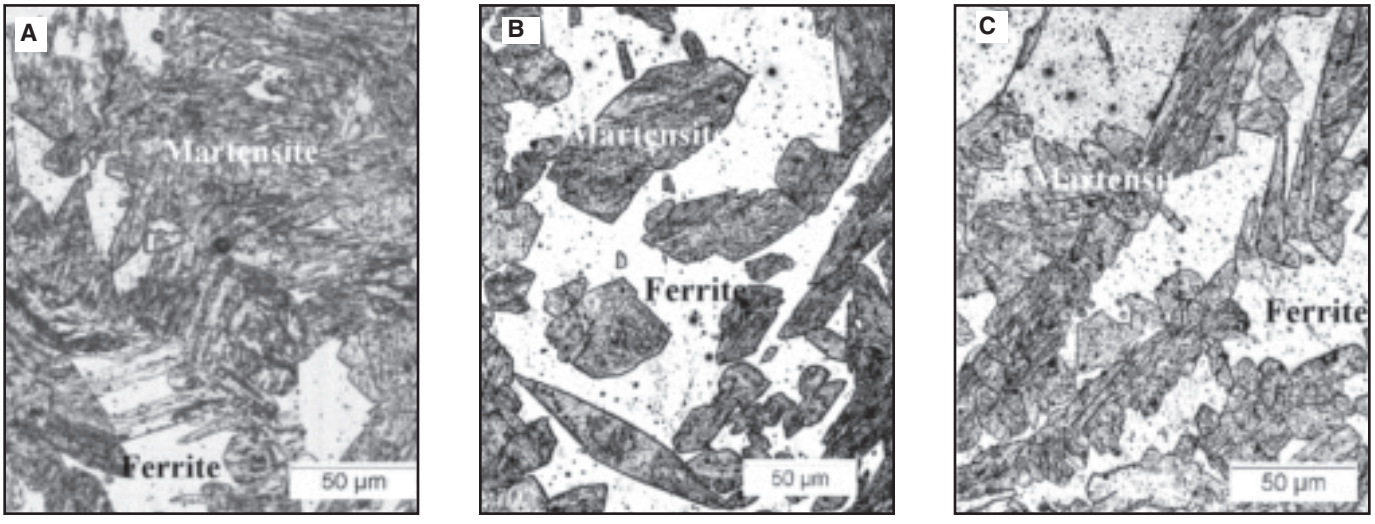

Fig. 15 — Microstructure of as-solidified fourth, fifth, and sixth passes in the A6 weld. A — As-solidified fourth pass, HV354; B — as-solidified fifth pass, HV258.5; C — as-solidified sixth pass, HV228.5.

indicate that tensile residual stresses will result in the welded joint. The characteristics of the microstructures will be discussed later.

Table 2 shows the summary of the dilatometric analysis.

Comparison between Measured and Predicted Ms Temperatures

Experimentally measured martensite transformation temperatures (T_{Ms}) of the designed wires are listed in Table 3, which also contains the T_{Ms} temperatures as estimated using the Self-Olson equation (Refs. 17, 18) and the Ghosh-Olson methodology (Refs. 19–21). The temperature of the conventional wire, ER70S-3, indicates ferrite transformation start temperature (T_{Fs}).

As can be seen in Table 3, the Ghosh and Olson methodology appears to better predict the T_{Ms} temperatures for these experimental alloys. Since the Self-Olson Equations were derived statistically based on a number of alloys, this equation is expected to provide more accurate results for alloys whose compositions fall within the range of the database.

Weld Microstructure

Comparison of Microstructure between Single-Pass and Gleeble Specimen

Figures 5–8 are micrographs of the single-pass weld beads and the Gleeble specimens from each of the designed wires. All were martensitic in nature. However, the two microstructures, i.e., single-pass weld and Gleeble specimen, are slightly different because the Gleeble specimens were extracted from bead-on-bead (BOB) welds, which experienced multiple thermal cycles.

Figure 9 shows the microstructures of the ER70S-3 single-pass weld bead and the Gleeble specimen. Ferrite clearly predominated in the microstructure. More specifically, acicular ferrite and grain boundary ferrite veining were the two major features observed in the single-pass weld while 100% polygonal ferrite was found in the Gleeble specimen.

The volume percents of the matrix microstructure (white in the figures) and carbides (black or gray) were determined

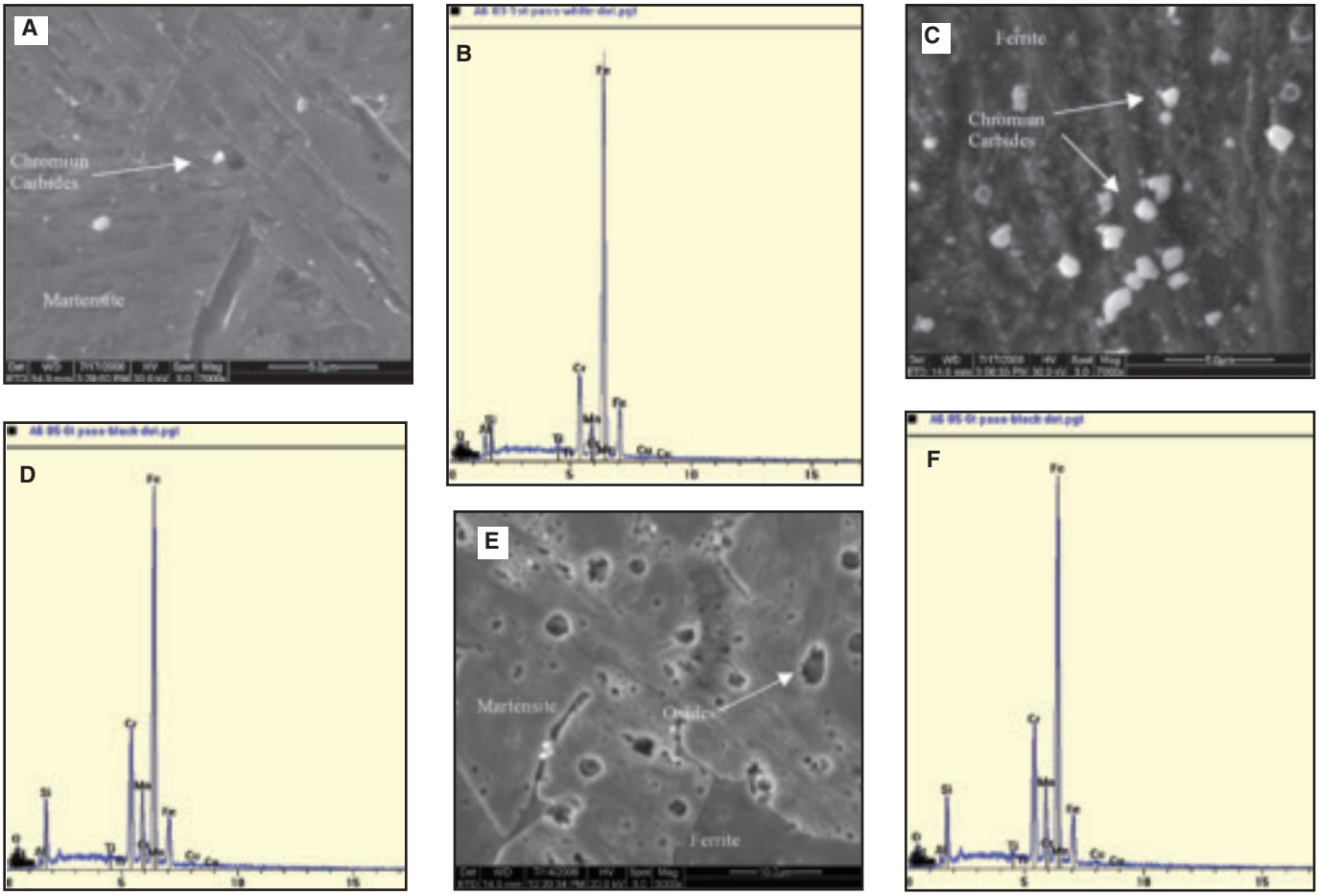

Fig. 16 — SEM micrographs and EDS analysis of weld A6. A — SEM image in the first pass; B — EDS result in the first pass; C — SEM image in the fourth pass; D — EDS result in the fourth pass; E — SEM image in the sixth pass; F — EDS result in the sixth pass.

using the point counting technique. The results for the single-pass welds and the Gleeble specimens are listed in Table 4.

Hardness profiles were measured on the dilatometric specimens and single-pass weldments. The average hardness readings are listed in Table 5. All readings corresponded to martensitic microstructure. Comparing the hardness test results from the actual single-pass welds, the values of the Gleeble specimens were lower, again due to the multiple thermal cycles experienced.

Microstructure of Multipass Weld Specimens

Characterization of the weld metal and reheated zone microstructures of the welds is described in this section. A macrophotograph of the three layer (six-pass B5) weldment is shown in Fig. 10. The solid lines trace the weld interfaces of each individual bead, identified by numbers; 1 indicates the first bead and 6 indicates the sixth bead. As shown in Fig. 11, the weldment was composed of three zones: a) as-solidified zone marked "As-S," b) once-reheated zone marked "1-RH," and c) twice-reheated zone named "2-RH."

Multipass Weld A1

Figure 12A and B show the as-solidified microstructure in the fifth pass and the once-reheated microstructure in the fourth pass, respectively. The as-solidified weld metal, Fig. 12A, was fully martensitic with a hardness reading of 383 on the Vickers scale. The reheated weld metal in Fig. 12B showed martensite and bainite, with an average hardness of HV292, which is lower than that measured in a fully martensitic microstructure. Bainite formed as a result of tempering.

Figure 13A and B show the microstructures of twice-reheated regions. These microstructures are more bainitic as compared to that of the single-reheated regions. The lower hardness values of 288 and 248 confirm the effect of multiple thermal cycles.

Multipass Weld A6

Figure 14A, B, and C show the micrographs of as-solidified first pass, second pass, and third pass, respectively, all with fully martensitic microstructure. Since carbon is low in these welds, the martensite is lathy in nature.

Different from the first, second, and third pass, the as-solidified fifth and sixth passes did not show 100% martensite in the microstructure. Instead, the martensite appeared as islands in the ferrite matrix as shown in Fig. 15A–C. These morphologies are similar to those reported in the literature, which described the undiluted microstructure of a weld metal of Type 403 martensitic stainless steel that contained 0.11% C, 12.38% Cr, and 0.28% Ni (Ref. 23). The amount of martensite in A6 wire weld was less than that of a type 403 stainless steel weld due to the lower carbon content of A6. The appearance of ferrite together with martensite will be explained in the next section on EDS analysis results.

Figure 16A shows an SEM photograph of the as-solidified first pass. Some isolated carbide particles are observed in the martensitic microstructure. EDS analysis in Fig. 16B showed Cr, Si, Ti, Mn, Al, and

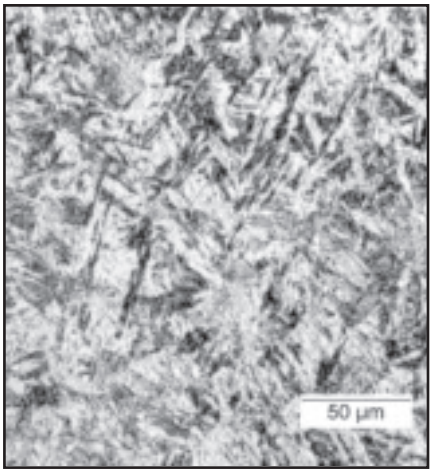

Fig. 17 — Martensitic microstructure of as-solidified first pass in weld B5.

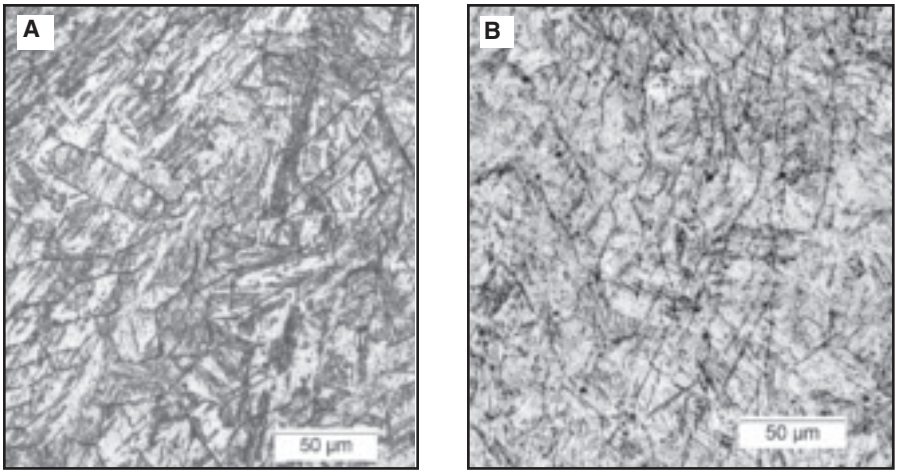

Fig. 18 — Microstructures of as-solidified and once-reheated areas. A — As-solidified sixth pass; B — once-reheated fifth pass.

Fe in the carbides. During welding, the first pass is expected to be more affected by dilution from the base steel. As such, the as-solidified first pass weld metal transformed into martensite because of carbon pickup from the base metal. On the contrary, in the later passes, weld metals contained less carbon and therefore martensite plus ferrite microstructures appeared. Figure 16C shows the SEM photograph of the as-solidified fourth pass, in which the effect of dilution was reduced. Larger carbide particles can be observed in the ferrite microstructure than in the first pass. The carbides were composed of Cr, Ti, Mn, and Fe. As a result of carbide precipitation, a carbon-depleted zone is expected to form around the carbides. The lower carbon content would then result in the formation of ferrite around the carbide particles. The ferrite next to the carbide precipitates in Fig. 16C confirms the explanation above.

On the other hand, many oxides composed of Si, Cr, Mn, Al, and Fe were observed in the as-solidified sixth pass in which little dilution of the base steel occurred, as shown in Fig. 16E. With the lower carbon in this region, the microstructure became ferrite and martensite as shown in Fig. 15B. High hardness values (above 300) resulted in these regions when the indent was located on the martensite even the regions were reheated. On the contrary, when the indent was on the ferrite matrix, the hardness values would be low.

Multipass Weld B5

Figure 17 shows the microstructure of the as-solidified first pass of weld B5. The microstructure is fully martensite with Vickers hardness reading of 398. The high hardness was believed to also be a result of base metal dilution as in the case of weld A6.

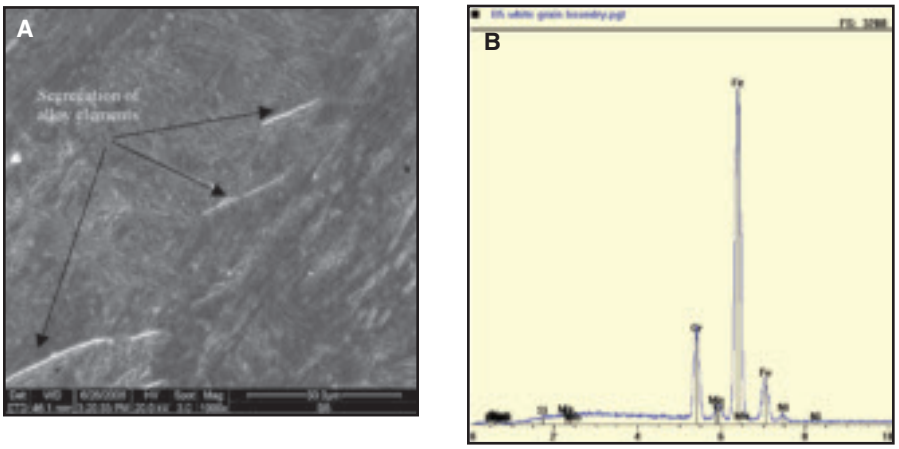

Fig. 19 — SEM and EDS analysis showing alloying element segregation along the grain boundaries. A — SEM photograph; B — EDS result.

Figure 18A and B show the as-solidified microstructure in the sixth pass and the once-reheated microstructure in the fifth pass, respectively. Figure 18A shows a martensitic microstructure with a Vickers hardness value of 368 while the reheated weld metal microstructure in Fig. 18B was bainitic with a hardness reading of $HV_{300}275$. The grain boundaries were clearly visible in both microstructures.

Figure 19 is a SEM photograph of the grain boundaries shown in Fig. 18. EDS analysis performed on the grain boundaries in Fig. 19B showed Cr, Mn, and Ni segregation. Chemical etching clearly developed the grain boundaries because of the alloying element segregation.

Multipass Weld C5

Figure 20A–D shows the microstructures of C5 weld beads. All of them were martensite, with hardness readings between 350 and 380, even in the reheated regions.

As expected, weld metal microstructures, whether single pass or multipass, are a result of chemical composition and thermal history. Base metal dilution, in this study, promoted the composition gradient, in particular, carbon, from the first pass to the later passes, as well as the hardness variations. The top beads with lower carbon exhibited a mixture of ferrite and martensite, and lower hardness readings. In terms of residual stress control, single-pass welds that had the correct chemical compositions demonstrated great ability to mitigate tensile residual stresses. Martensite started at a low temperature and ended close to room temperature. The effect of multipass welds on residual stress control is more difficult to assess because of the pass-to-pass chemical composition dilution and the prior bead thermal history. Thus, residual stress control via martensite transformation should be designed for structures with joints that can be accomplished through single-pass welding.

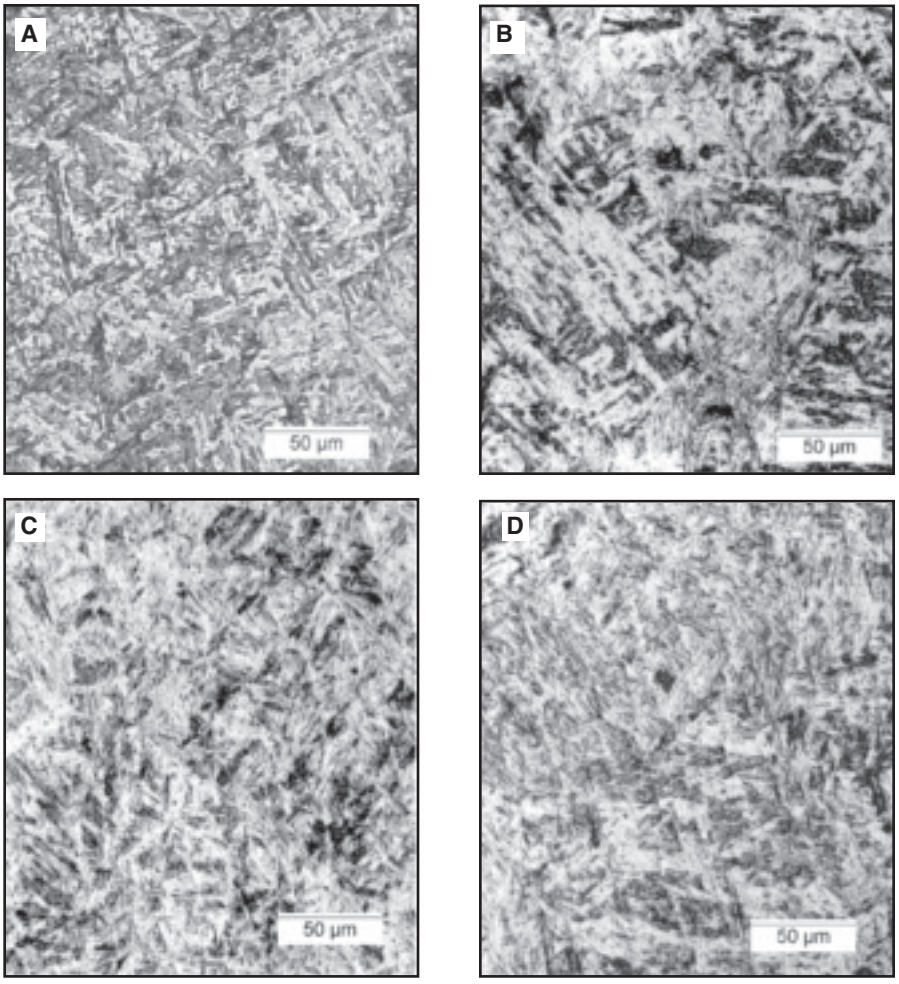

Fig. 20 — Microstructures of C5 weld beads. A — As-solidified sixth pass; B — once-reheated first pass; C — once-reheated fifth pass; D — twice-reheated with the fourth and sixth passes.

Conclusions

The low-transformation-temperature welding (LTTW) consumables design in this investigation exhibited expansion during cooling in a weld thermal cycle. Therefore, the experimental electrodes with lower Cr-Ni contents are capable of promoting compressive residual stresses in welds. Chemical composition proved to be critical in determining the martensite start temperature and martensite transformation behavior. Base metal dilution regarding carbon must be limited to maximize martensite formation. Weld joints designed to use single beads will be optimal for residual stress control. The major finding of this research is listed below.

- Martensite transformation start temperatures of the four designed wires are 390°C for A1, 360°C for A6, 300°C for B5, and 270°C for C5. The commercial wire, ER70S-3, transforms into ferrite at 645°C.
- Expansive strains developed for the designed wires in the dilatometric testing. The amount of the expansive strains for B5 and C5 are larger than those of A1 and A6. The expansion resulted in a compressive stress state. On the contrary, contractive strains and tensile residual stress resulted for the commercial E70S-3 wire.
- In single-pass welding, the microstructures of the designed wires are martensite due to the high chromium and/or nickel content of the experimental electrodes as well as carbon dilution of the base steel.
- The microstructure of the Gleeble specimen for all designed wires was martensitic.
- The microstructures of multipass A6 welds are martensite in the first to fourth passes, where dilution exerts the greatest effect; those in the fifth and sixth passes are composed of martensite and ferrite.
- The microstructures of multipass B5 welds are mainly martensite. Some alloy elements such as Cr, Ni, and Mn are observed to segregate along the grain boundaries.
- The microstructures of multipass C5 welds are fully martensite with microhardness reading between 350 and 380, even in the reheated regions.

Nomenclature

e_α = Thermal expansion coefficient of ferrite
e_γ = Thermal expansion coefficient of austenite
T_0 = Equilibrium austenite decomposition temperature
T_{Ff} = Ferrite finish temperature
T_{Fs} = Ferrite start temperature
T_{Ms} = Martensite transformation start temperature
T_{Mf} = Martensite finish temperature
ΔT_m = Undercooling range for the austenite-to-martensite transformation
Ac_1 = Temperature at which austenite begins to form during heating
Ac_3 = Temperature at which transformation of ferrite to austenitic is completed
during heating.

Acknowledgments

Author M. C. Payares-Asprino would like to thank the Venezuelan Science and Technology Research Foundation (FONACIT) and the Colorado School of Mines–Center for Welding, Joining and Coatings Research (CSM-CWJCR) for the financial and research support. Author H. Katsumoto acknowledges the support of Sumitomo Metals Co. for the sabbatical research at CSM-CWJCR.

References

1. *Metals Handbook*, 9th Ed., Vol. 6, Welding, Brazing, and Soldering. 1983. ASM International, Materials Park, Ohio.
2. Mochizuki, M., Hattori, T., and Nakakado, K. 2000. Residual stress reduction and fatigue strength improvement by controlling welding pass sequences. *Journal of Engineering Materials and Technology* 122: 108–112.
3. Löhe, D., Lang, K. H., and Vöhringer, O. 2002. Residual stress and fatigue behavior. *Handbook of Residual Stress and Deformation of Steel*. G. Totten, M. Howes, and T. Inoue, editors. ASM International, Materials Park, Ohio, pp. 27–53.
4. Lu, J. 2002. Prestress engineering of structural material: A global design approach to the residual stress problem. *Handbook of Residual Stress and Deformation of Steel.* G. Totten, M. Howes, and T. Inoue, editors. ASM International, Materials Park, Ohio, pp. 11–26.
5. Withers, P. J., and Bhadeshia, H. K. D. H. 2001. Residual stress Part I – Measurement techniques. *Materials Science and Technology* 17: 355–365.
6. Withers, P. J., and Bhadeshia, H. K. D. H. 2001. Residual stress Part II – Nature and origins. *Materials Science and Technology* 17: 366–375.
7. Jones, W. K. C., and Alberry, P. J. 1977.

Metals Technology 11: 557–566.

8. Ohta, A., Watanabe, O., Matsuoka, K., Maeda, Y., Suzuki, N., and Kubo, T. 2000. Fatigue strength improvement of box welds by low transformation temperature welding wire and PWHT. *Welding in the World* 44(3): 19–23.

9. Eckerlid, J., Nilsson, T., and Karlsson, L. 2003. Fatigue properties of longitudinal attachments welded using low transformation temperature filler. *Science and Technology of Welding and Joining* 8(5): 353–359.

10. Martinez, F., and Liu, S. 2006. Development of compressive residual stress in structural steel weld toes by means of weld metal phase transformations. *Proc. of the Trends in Welding Research Conference*, pp. 583–588, Pine Mountain, Ga., May 2005, published in August 2006.

11. Martinez-Diez, F. 2007. The development of a compressive residual stress field around a weld toe by means of phase transformations. IIW Granjon Award, *Welding in the World*.

12. Castro, R., and de Cadenet, J. J. 1975. *Welding Metallurgy of Stainless and Heat-Resisting Steels.* Cambridge University Press, Cambridge, UK.

13. Porter, D. A., and Easterling, K. E. 1992. *Phase Transformations in Metals and Alloys*. CRC Press, London, UK.

14. Hornbogen, E. 1985. The effect of variables on martensitic transformation temperature. *Acta Metallurgica* 33(4): 595–601.

15. Kaufmann, L. 1963. *Solids under Pressure.* W. Paul and D. M. Warschauer, editors. New York, N.Y.: McGraw-Hill Book Co., Inc.

16. Izumiyama, M., Tsuchiya, M., and Imai, Y. 1974. *Journal of Japan Institute of Metallurgy* 34: 291.

17. Liu, Y. X. 1991. *Principle of Heat Treatment.* China Mechanical Industries Press, Beijing, China.

18. Self, J. A., Olson, D. L., and Edwards, G. R. 1987. The stability of austenitic weld metal. *NBS Publication on Cryogenic Properties of Metals*, pp. 181–189.

19. Self, J., Matlock, D. K., and Olson, D. L. 1984. An evaluation of austenitic Fe-Mn-Ni weld metal for dissimilar metal welding. *Welding Journal* 63(9): 282-s to 288-s.

20. Ghosh, G., and Olson, G. B. 1994. Kinetics of F.C.C.→B.C.C. Heterogeneous martensitic nucleation-I, The critical driving force for athermal nucleation. *Acta Metallurgica et Materialia* 42: 3361–3370.

21. Ghosh, G., and Olson, G. B. 1994. Kinetics of F.C.C.→B.C.C. Heterogeneous martensitic nucleation-II, Thermal activation. *Acta Metallurgica et Materialia* 42: 3371–3379.

22. Ghosh, G., and Olson, G. B. 2002. The isotropic shear modulus of multicomponent Fe-base solid solutions. *Acta Metallurgica et Materialia* 50: 2655–2675.

23. Balmforth, M. C., and Lippold, J. C. 1998. A preliminary ferritic-martensitic stainless steel constitution diagram. *Welding Journal* 77(1): 1-s to 6-s.

24. Darcis, Ph. P., Katsumoto, H., Payares-Asprino, M. C., Liu, S., and Siewert, T. A. 2007. Cruciform fillet welded joint fatigue strength improvements by weld metal phase transformations. *Intl. Journal of Fatigue and Fracture of Engineering Materials and Structures*, doi: 10.1111/j.1460-2695.2007.01205.x, November.

Statement of Ownership, Management and Circulation for U.S. Postal Service (Required by U.S.C. 3685)

1. TITLE OF PUBLICATION: Welding Journal 2. PUBLICATION NO.: ISSN 0043-2296
3 DATE OF FILING: September 16, 2008 4. FREQUENCY OF ISSUE: Monthly
5. NO. OF ISSUES PUBLISHED ANNUALLY: 12 6. ANNUAL SUBSCRIPTION: $120.00
7. MAILING ADDRESS OF KNOWN OFFICE OF PUBLICATION: 550 N.W. LeJeune Rd., Miami, Dade County, Florida 33126
8. MAILING ADDRESS OF THE HEADQUARTERS OR GENERAL BUSINESS OFFICES OF THE PUBLISHERS:
550 NW LeJeune Rd., Miami, Dade County, Florida 33126
9. NAMES AND COMPLETE ADDRESS OF PUBLISHER, EDITOR AND MANAGING EDITOR:
PUBLISHER: Andrew Cullison, AWS, 550 NW LeJeune Rd., Miami, Florida 33126
EDITOR: Mary Ruth Johnsen, AWS, 550 NW LeJeune Rd., Miami, Florida 33126
10. OWNER: NAME: American Welding Society,Inc. ADDRESS: 550 NW LeJeune Rd., Miami, Florida 33126
11. KNOWN BONDHOLDERS, MORTGAGEES, AND OTHER SECURITY HOLDERS OWNING OR HOLDING 1 PERCENT OR MORE OF TOTAL AMOUNT OF BONDS, MORTGAGES OR OTHER SECURITIES: None
12. The purpose, function, and nonprofit status of this organization and the exempt status for Federal income tax purposes: Has not changed during preceding 12 months
13. Publication Title: Welding Journal 14. Issue date for Circulation Data Below: October 2008
15. EXTENT AND NATURE OF CIRCULATION:

	Average No. Copies Each Issue During Preceding 12 Months	Actual No.Copies of Single Issue Published Nearest to Filing Date
A. Total No. Copies Printed (Net Press Run)	55,685	56,225
B. Paid and/or Requested Circulation		
1. Paid / Requested Outside-County Mail Subscriptions Stated on Form 3541	53,395	54,102
2. Paid In-County Subscriptions Stated on Form 3541	None	None
3. Sales Through Dealers and Carriers, Street Vendor, Counter Sales, and other Non-USPS Paid Distribution	None	None
4. Other Classes Mailed Through the USPS	None	None
C. Total Paid / Requested Circulation	53,395	54,102
D. Free Distribution by Mail (Samples, complimentary and other free)		
1. Outside-County as State on Form 3541	418	410
2. In-County as Stated on Form 3541	None	None
3. Other Classes Mailed Through the USPS	None	None
4. Free Distribution Outside the Mail (Carriers or other means)	None	None
E. Total Free Distribution	418	410
F. Total Distribution	53,813	54,512
G. Copies not Distributed	1,872	1,713
H. Total	55,685	56,225
I. Percent Paid and / or Requested Circulation	99.2%	99.2%

16. Statement of Ownership will be printed in the November 2008 issue of this publication.
I certify that the statements made by above are correct and complete:
Andrew Cullison, Publisher

Welding Journal 2009 Editorial Calendar

Editorial Profile

For those engaged in welding-related activities, *Welding Journal* provides current news, features, research reports, practical data, and advertisements from industry leaders around the world. Also featured are welding-related metalworking activities such as design, testing and inspection, maintenance and repair, and training.

Other Editorial Features of *Welding Journal*

- News of the Industry
- New Products
- New Literature
- Aluminum Q&A
- Welding Workbook
- Washington Watchword
- Brazing Q&A
- Peer-Reviewed Welding Research
- Book Reviews
- Press Time News
- Society News
- Personnel
- Editorial
- Soldering Topics
- Stainless Steel Q&A
- Coming Events
- International Update
- Resistance Welding Q&A

		Editorial Deadline	Advertising Deadline
January	• GMAW: Tips for Good Welds • 2008 FABTECH Int'l & AWS Welding Show Review	November 21, 2008	December 2, 2008
February	• Welding in the Aerospace Industry • Torches and Welding Guns Update	December 19, 2008	January 2, 2009
March	• What's Happening with the Welding of Plastics • Laser Beam Welding and Cutting • **Bonus:** The American Welder	January 23	February 2
April	• Brazing and Soldering Today • Matching Filler Metals to the Base Metal	February 20	March 2
May	• Welding in the Nuclear Power Industry • Pipe and Tube Welding	March 23	April 2
June	• Special Celebration: AWS's 90th Anniversary • GMAW: Tips for Good Welds	April 20 *Free Readership Survey for Advertisers*	May 4
July	• Career Opportunities in the Welding Field • Thermal Spray Applications	May 22	June 1
August	• Manufacturing for a "Green" World • Essen Welding Fair Preview • NDE Update	June 22 *Bonus Distribution: Essen Welding and Cutting Fair*	July 2
September	• Understanding Weld Cracking • Welding in the Shipbuilding Industry • **Bonus:** The American Welder	July 24	August 3
October	• Brazing and Soldering Today • A Look at Aluminum Welding	August 21	September 2
November	• FABTECH Int'l & AWS Welding Show Preview	September 21 *Bonus Distribution: FABTECH Int'l & AWS Welding Show*	October 1
December	• Resistance Welding Developments • Selecting Personal Protective Equipment	October 22	November 2